Evidence for shape coexistence in ^{98}Mo

T. Thomas,[1,2,*] K. Nomura,[1,3] V. Werner,[2] T. Ahn,[2] N. Cooper,[2] H. Duckwitz,[1] M. Hinton,[2,4] G. Ilie,[2] J. Jolie,[1] P. Petkov,[1,5] and D. Radeck[1]

[1]*Institut für Kernphysik, Universität zu Köln, Zülpicher Straße 77, D-50937 Köln, Germany*

[2]*Wright Nuclear Structure Laboratory, Yale University, New Haven, Connecticut 06520, USA*

[3]*Grand Accélérateur National d'Ions Lourds, CEA/DSM-CNRS/IN2P3, Boulevard Henri Becquerel, F-14076 Caen Cedex 05, France*

[4]*Department of Physics, University of Surrey, Guildford GU2 7XH, United Kingdom*

[5]*Bulgarian Academy of Science, Institute for Nuclear Research and Nuclear Energy, Tsarigradsko Chausse 72, 1784 Sofia, Bulgaria*

(Received 6 June 2013; revised manuscript received 5 September 2013; published 7 October 2013)

A $\gamma\gamma$ angular-correlation experiment has been performed to investigate the low-energy states of the nucleus ^{98}Mo. The new data, including spin assignments, multipole mixing ratios, and lifetimes reveal evidence for shape coexistence and mixing in ^{98}Mo, arising from a proton intruder configuration. This result is reproduced by a theoretical calculation within the proton-neutron interacting boson model with configuration mixing, based on microscopic energy density functional theory. The microscopic calculation indicates the importance of the proton particle-hole excitation across the $Z = 40$ subshell closure and the subsequent mixing between spherical vibrational and the γ-soft equilibrium shapes in ^{98}Mo.

DOI: 10.1103/PhysRevC.88.044305 PACS number(s): 21.60.Jz, 21.60.Fw, 23.20.En, 25.55.−e

I. INTRODUCTION

For decades, clarifying the nature of shape coexistence has been one of the major objectives in nuclear structure physics [1,2]. The phenomenon has been observed in various regions of the nuclear chart, from light [3] to heavy [4] systems. In ^{186}Pb, for example, three low-lying 0^+ states bunch together in energy within the range of 700 keV [4]. The emergence of the extremely low-lying 0^+ states is, in terms of the spherical shell model, attributed to two- or four-proton excitations across the $Z = 82$ shell closure. The residual interaction between protons and neutrons leads to the lowering of the excited 0^+ states and the different corresponding shell-model configurations are linked to relevant geometrical deformations in a mean-field picture [5].

The $A \sim 100$ mass region also presents a unique laboratory for the evolution of nuclear shape and shape coexistence [6,7]. The interplay between single-particle and collective degrees of freedom leads to shape phase transitions along isotopic and isotonic chains [8]. The most dramatic examples for shape coexistence and shape transition occur in the Zr isotopic chain, as recently revealed for ^{94}Zr [9]. Especially in the $N = 50$–56 Zr isotopes the 0^+_1 state and the very low-lying 0^+_2 state are considered strongly mixed $0p$-$0h$ and $2p$-$2h$ proton configurations, where protons are promoted from the pf shell to the $g_{9/2}$ orbital, as also found in shell-model calculations [6,10]. The structure of the low-lying 0^+_2 state in $N \geqslant 58$ Zr isotopes is somewhat more complicated due to neutron contributions. In Mo isotopes, starting from $N = 50$, the nuclear shape gradually evolves from a sphere and, driven by the enhanced proton-neutron residual interaction, large deformation sets in at $N \approx 60$ [11]. Situated in between, $^{98}_{42}$Mo$_{56}$ is pivotal for understanding shape transitions in this mass region. In particular, the concept of shape coexistence can apply to this nucleus, where proton cross-shell excitations from the $Z = 28$–40 pf shell to the $\pi g_{9/2}$ orbit may play an important role [12]. In fact, experimentally, the first-excited state of ^{98}Mo has been shown to be an coexisting isomeric 0^+ state of different shape [13,14]. The mixing between the proton $2p$-$0h$ and $4p$-$2h$ configurations forms the first excited 0^+ state and the ground state as revealed by the investigation of γ transitions depopulating 1^+ states with equal strengths to both 0^+ states [12], akin to the findings for ^{92}Zr [6].

To address the important issue of the nature of low-lying structure in ^{98}Mo, we performed a $\gamma\gamma$ angular-correlation experiment. In this paper, the results of this experiment are reported as well as the identification of shape coexistence and the role of a proton intruder configuration in ^{98}Mo. The experimental results are supported by predictions of the interacting boson model [15] with configuration mixing, where the Hamiltonian is determined microscopically. The microscopic calculation indicates the importance of the proton intruder configuration and the substantial mixing between spherical-vibrational and γ-unstable shapes in ^{98}Mo.

II. EXPERIMENTAL PROCEDURE

In order to extend the ^{98}Mo level scheme, we used the reaction ^{96}Zr(α, $2n$)^{98}Mo. A 16 MeV α beam was delivered by the extended stretched transuranium (ESTU) tandem accelerator at the Wright Nuclear Structure Laboratory, Yale University, impinging on a 1.25 mg/cm^2 thick ^{96}Zr target enriched to 57.36%. The γ transitions were detected by 10 Compton-suppressed high-purity Ge (HPGe) Clover detectors of the YRAST Ball array [16]. During five days of measurement, 1.2×10^9 events were collected using a $\gamma\gamma$ coincidence trigger.

Figure 1 shows the total projection of the $\gamma\gamma$ coincidence data. Due to impurities in the ^{96}Zr target transitions from $^{93–99}$Mo isotopes were observed. The most prominent peaks are labeled with their associated nuclear origin. The data

*tim.thomas@ikp.uni-koeln.de

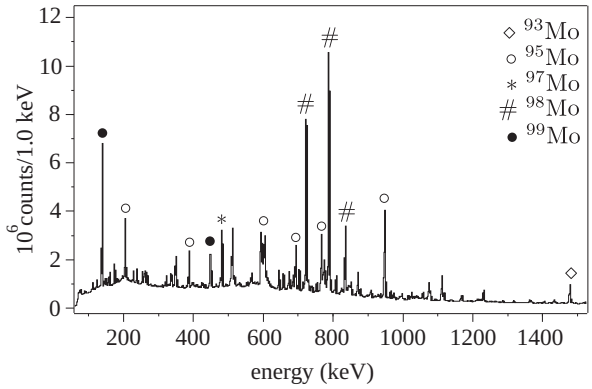

FIG. 1. Total projection of the $\gamma\gamma$ coincidence data. Major peaks from ^{98}Mo and the main side reactions are marked.

were sorted into 11 correlation group matrices, which account for detector pairs at angles Θ_1 and Θ_2 with respect to the beam axis and a relative angle ψ between the plains spanned by the detectors and the beam axis, in order to perform a $\gamma\gamma$ angular-correlation analysis. Relative intensities in the correlation groups were then fit to angular-correlation functions to extract spins and multipole mixing ratios, as described in Refs. [17,18], by using the computer code CORLEONE [19,20]. The code takes into account the attenuation factors of the detectors [21,22]. An example of a $\gamma\gamma$ angular-correlations analysis is shown in Fig. 2 for the $2_4^+ \xrightarrow{1419} 2_1^+ \xrightarrow{787} 0_{gs}^+$ cascade, yielding the hitherto unknown multipole mixing ratio $\delta_{1419} = 0.33 \pm 0.11$. In the literature [23], conflicting multipole mixing ratios are given for γ transitions depopulating low-lying states in ^{98}Mo. The superior sensitivity of the present setup allowed us to resolve discrepancies. For more detailed information about $\gamma\gamma$ angular-correlations analysis with the YRAST Ball array see Refs. [22,24]. In the same way, the multipole mixing ratio of the $2_2^+ \xrightarrow{644} 2_1^+$ transition was measured to be $+1.67\,(25)$, which is in agreement with the larger solution from an $(n, n'\gamma)$ experiment [25] and refutes the most recent value from Coulomb excitation [14].

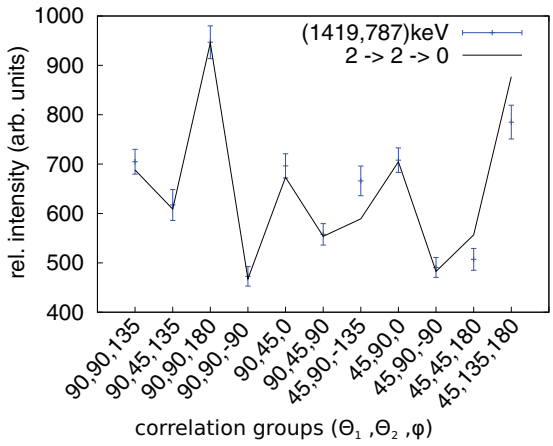

FIG. 2. (Color online) Comparison of a fitted theoretical angular correlation (solid line) with relative intensities obtained from 11 correlation groups for the 1419–787 keV $\gamma\gamma$ coincidence.

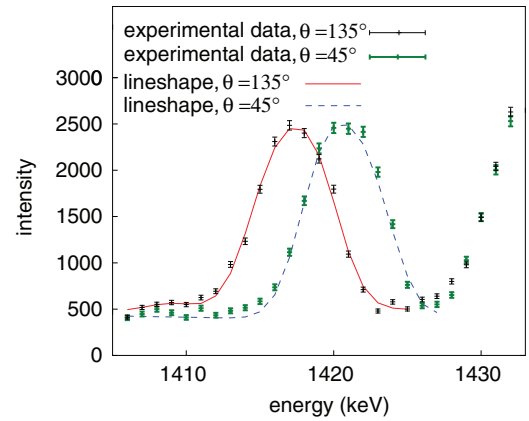

FIG. 3. (Color online) Determination of the effective lifetime of the 1419 keV transition depopulating the 2_4^+ state using a gate set on the 787 keV transition. Coincidence spectra with a gate set on the 787 keV transition for two different angles are shown. The red solid line represents the simulated lineshape at forward angle and the blue dashed line the backward angle. The effective average lifetime is $\tau = 0.30\,(7)$ ps.

Lifetimes of excited states were determined using the Doppler-shift attenuation method (DSAM) [26]. The data was sorted into three matrices according to the three angles $\theta = 45^\circ$, 90°, 135° of the detectors relative to the beam axis. For the lineshape analysis, the stopping process of an excited nucleus is simulated using nuclear [27] and electronic stopping powers [28]. In Fig. 3, a lineshape analysis for the 1419 keV transition depopulating the 2_4^+ state is shown. The weighted mean value over the angles for the effective lifetime is calculated to be $\tau = 0.30\,(7)$ ps. The analysis procedure is outlined in more detail in Ref. [29].

III. THEORETICAL PROCEDURE

To interpret the nature of the low-lying structure and the relevant shape dynamics in ^{98}Mo, we performed a self-consistent mean-field calculation using the Skyrme energy density functional (EDF) (see Ref. [30] for review). Figure 4(a) shows the total energy surface of ^{98}Mo in terms of the axial quadrupole deformation β and triaxiality γ [31] obtained through the constrained Hartree-Fock-BCS (HF-BCS) method with the Skyrme functional SLy6 [32] using the code EV8 [33]. Figure 4(a) displays two minima in the mean-field energy surface, with the deeper one being close to a spherical shape ($\beta \approx 0$) and the other at $\beta \approx 0.21$ and $\gamma \approx 20^\circ$ with some degree of softness. On the other hand, no coexisting minima are visible in the microscopic energy surfaces of the adjacent nuclei ^{96}Mo [Fig. 4(c)] and ^{100}Mo [Fig. 4(d)]. ^{98}Mo appears to be transitional between near-spherical (^{96}Mo) and deformed (^{100}Mo) shapes.

To study quantitatively the spectroscopic observables associated with the intrinsic shape of interest, it is necessary to go beyond the mean-field approximation. In this work we resort to the proton-neutron interacting boson model (IBM-2) [15,34] to generate spectra and transition rates that are comparable to data. By mapping the microscopic energy surface onto the

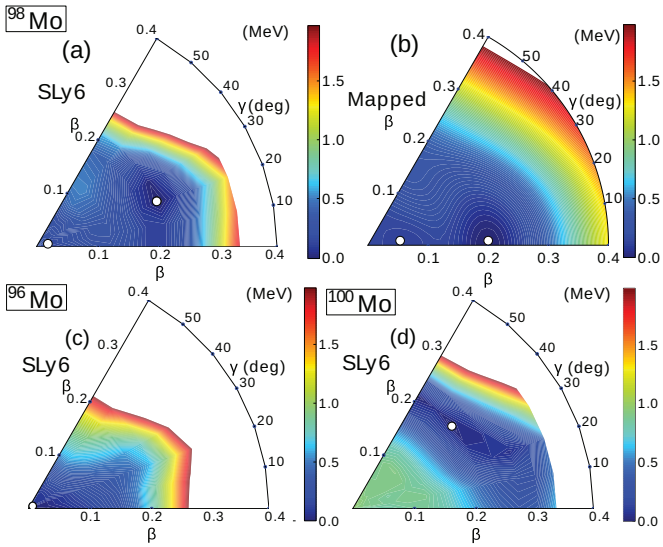

FIG. 4. (Color online) Contour plots of the microscopic (a) and the mapped (b) energy surfaces in (β, γ) plane of ^{98}Mo, and of the microscopic energy surfaces of the adjacent nuclei ^{96}Mo (c) and ^{100}Mo (d). The color code ranges from 0 (mean-field minimum) to 2 MeV, and the minima are identified by the solid white circles. The Skyrme SLy6 functional is used.

equivalent IBM-2 Hamiltonian in the boson condensate [35], the Hamiltonian parameters are determined microscopically, thereby not invoking any adjustment to data (cf. Refs. [36,37] for details). The mapped Hamiltonian is to be diagonalized numerically in the boson m-scheme basis to provide level energies and transition rates with good quantum numbers in the laboratory frame. We note that the above-mentioned procedure is similar to that used in Ref. [38], where it was used to make a prediction on the structure of ^{96}Kr, whereas in the present work we put this procedure to a more crucial test.

In order to describe the two mean-field minima, the model space of the IBM-2 needs to be extended by including the intruder configuration and by mixing the Hamiltonians associated with the two configurations [39]. From the observed systematics of the two-neutron separation energies (see, e.g., Ref. [40] for a review), the $N = 56$ neutron subshell gap is only notable for $Z \leqslant 40$, and the gap becomes rapidly quenched for higher Z ($\geqslant$42). This indicates that proton intruder states are more significant for heavier Mo isotopes than neutron shell effects. Furthermore, the calculated single-particle energies as functions of the β deformation indicate the lowering of the proton $g_{9/2}$ orbitals and the occupation of the last protons in the orbitals at $\beta \approx 0.2$ associated with the γ-soft minimum in Fig. 4(a). These considerations lead us to take the IBM-2 model space including the two-proton excitation across the $Z = 40$ shell. The ^{90}Zr nucleus is then taken to be the inert core, and the number of proton bosons is 1 and 3 for the normal and the intruder configurations, respectively, while the neutron boson number is fixed at 3. Note that normal (intruder) configuration denotes hereafter the proton $2p$-$0h$ ($4p$-$2h$) configuration. The full Hamiltonian of the system is then given as [38]

$$H = P_{\rm nor} H_{\rm nor} P_{\rm nor} + P_{\rm intr}(H_{\rm intr} + \Delta) P_{\rm intr} + H_{\rm mix}, \qquad (1)$$

TABLE I. The intrinsic deformation parameter β_2 for the lowest-three excited 2^+ states. The theoretical values extracted from the intrinsic quadrupole moments obtained by the IBM-2 ($K = 0$ is assumed) $\beta_2^{\rm IBM}$, and the equivalent values $\beta_2^{\rm MF}$ associated with the mean-field minima, and the experimental values $\beta_2^{\rm expt}$ from inelastic scattering of deuterons [43,44] and Coulomb excitation [45] are shown.

$E_{\rm level}$ (keV)	J^π	$\beta_2^{\rm MF}$	$\beta_2^{\rm IBM}$	$\lvert\beta_2^{(d,d')}\rvert$	$\lvert\beta_2^{\rm CoulEx}\rvert$[a]
787.26	2_1^+	(+0.21)	+0.132	0.167 (4)[b]	0.174 (5)
1432.29	2_2^+	(≈0.0)	+0.060	0.046[c]	0.037 (2)
1758.32	2_3^+		− 0.121	0.029[c]	0.11 (5)

[a]Taken from Ref. [45].
[b]Taken from Ref. [44].
[c]Taken from Ref. [43].

where $H_{\rm nor}$ ($H_{\rm intr}$) and $P_{\rm nor}$ ($P_{\rm intr}$) represent the Hamiltonian of and the projection operator onto the normal (intruder) configuration space, respectively. Δ and $H_{\rm mix} = \omega(s_\pi^\dagger s_\pi^\dagger + d_\pi^\dagger d_\pi^\dagger) + {\rm H.c.}$ stand for the energy offset needed for the proton cross-shell excitation and interaction that mixes two configurations, respectively. The resulting mapped IBM-2 energy surface is shown in Fig. 4(b). One can see in Fig. 4(b) two equivalent minima near $\beta \approx 0$ and $\beta \approx 0.2$, with the latter being γ soft similarly to the microscopic energy surface.[1]

IV. RESULTS AND DISCUSSION

The calculation predicts a spectroscopic quadrupole moment for the 2_1^+ state of $Q(2_1^+) = -0.245e$b, corresponding to a weak prolate deformation. This is consistent with a previous experimental value of $Q(2_1^+) = -0.25\,(9)e$b [42], but differs from the more recent one, $Q(2_1^+) = -0.05\,(2)e$b [14]. We note that the latter result stems from a global fit to data taking known multipole mixing ratios and lifetimes into account. Some of these input data have been changed and complemented by our present measurement. In Table I, we give the intrinsic β-deformation parameters for the lowest three 2^+ states, taken from inelastic scattering [43,44] and Coulomb excitation [45] data. These data are compared to the value obtained from the minima in the mean-field energy surface [Fig. 4(a)], and the deformation extracted from the intrinsic quadrupole moment in the IBM-2, assuming $K = 0$. The best agreement is found with Coulomb excitation values from Ref. [45].

Next we analyze the structure of the low-energy level scheme of ^{98}Mo. Figure 5 compares the data from the present experiment (left-hand side) and the calculated spectra after (center) and before the mixing, i.e., unperturbed configurations (right-hand side). Note that some experimental states, which are close in energy and have the same spin, have been identified

[1]A minimum at $\gamma = 20^\circ$, however, is not obtained with the used Hamiltonian containing up to only two-body boson terms. It has been shown [41] that a three-body boson term should be included in the IBM Hamiltonian to give rise to the triaxial minimum and to better describe the detailed structure of the quasi-γ band. This is, however, not particularly of relevance for the present paper.

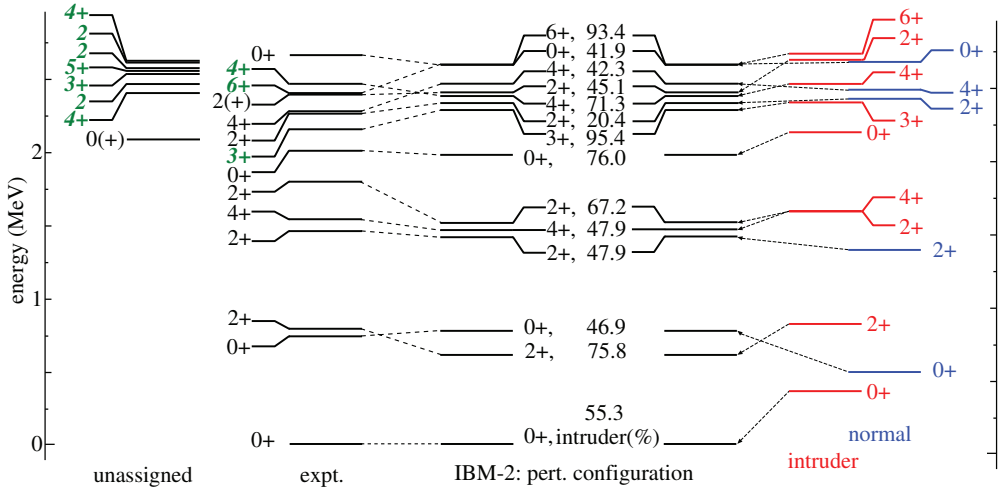

FIG. 5. (Color online) Low-energy level scheme of ^{98}Mo. The experimental (left) and the calculated spectra with mixing ("IBM-2: pert. configuration," center) and without mixing (right). New spin assignments are denoted in italic letters. The number indicated next to spin value (center) represents the fraction of the intruder configuration in the wave function of each state.

from the comparison to predicted B(E2) values (cf. Tables II and III). Even though the energy levels are calculated without any fit to data; that is, the Hamiltonian parameters are derived solely from the microscopic EDF and the mapping procedure, the overall agreement between data and calculation in Fig. 5 is remarkably good. While the experimental 0_2^+ excitation energy is well reproduced by the theory, the calculated 2_1^+ level energy seems rather low compared with the experimental value. The reason is the strong level repulsion between the unperturbed low-spin states of the two configurations due to a rather large mixing strength. In the experiment an excess of states is observed above the 0_4^+ state, which could not be assigned to predicted states. These might originate from a more complicated structure eventually associated with higher-order effects such as the four-proton cross-shell excitation and/or the excitation of neutrons, which are outside of the model space of the present calculation.

Looking into the origin of each state in a more quantitative manner, first we notice on the right-hand side of Fig. 5 that the unperturbed 0_1^+ and 0_2^+ states of the normal and the intruder configurations are very close in energy. After the mixing, the 0^+ ground states in each configuration repel each other by ≈350 keV in energy (as illustrated by arrows). Here, the matrix element $\langle H_{\rm mix}\rangle$, which mixes unperturbed 0_1^+ states of the normal and the intruder configurations, is calculated to be 385 keV. This value is consistent with the result from a schematic two-level mixing calculation of 326 keV [12]. In the resulting 0_1^+ and 0_2^+ states, normal and intruder configurations

TABLE II. Theoretical E2 transition strengths (in W.u.) compared to experimental values from Refs. [14,23] and from this work. States in bold are predicted to be of intruder nature in theory. For transitions with mixed multipolarity the multipole mixing ratio δ measured in the present experiment is given.

$E_{\rm level}$ (keV)	J_I^π	E_γ (keV)	J_F^π	B(E2)$_{\rm theor}$	B(E2)$_{\rm expt}$	$\delta_{\rm expt}$
787.26[a]	$\mathbf{2_1^+}$	787.26	$\mathbf{0_1^+}$	27	$21.4\,^{+11}_{-10}$	
		52.6	0_2^+	256	280 (40)[b]	
1432.29[a]	2_2^+	644.70	$\mathbf{2_1^+}$	22	47.8^{+132}_{-100}	+1.67 (25)
		697.10	0_2^+	8	2.5^{+8}_{-6}	
		1432.29	$\mathbf{0_1^+}$	0.03	1.0^{+2}_{-1}	
1509.74[a]	4_1^+	722.48	$\mathbf{2_1^+}$	49	$49.1^{+5.5}_{-4.5}$	
1758.32[a]	$\mathbf{2_3^+}$	326.05	2_2^+	13	4.7^{+189}_{-23}	−0.17 (22)
		971.03	$\mathbf{2_1^+}$	6	3.2^{+134}_{-16}	−0.97 (14)
		1023.61	0_2^+	7	7.8^{+286}_{-34}	
2206.74	2_4^+	1419.48	$\mathbf{2_1^+}$	1.3	1.7 (2)	−0.33 (11)
2333.03	$2_5^{(+)}$	900.85	2_2^+	1	1.6^{+8}_{-4}	$-0.15^{+0.19}_{-0.20}$
2343.26[c]	$\mathbf{6_1^+}$	833.52	4_1^+	56	10.1 (4)	

[a] τ Adopted from Ref. [45].
[b] B(E2) adopted from Ref. [23].
[c] τ Adopted from Ref. [14].

TABLE III. Same as Table II, but normalized with respect to the largest B(E2) value among the depopulating decays from a given initial state.

$E_{\rm level}$ (keV)	J_I^π	E_γ (keV)	J_F^π	B(E2)$^{\rm rel}_{\rm theor}$	B(E2)$^{\rm rel}_{\rm expt}$	$\delta_{\rm expt}$
1962.81	$\mathbf{0_3^+}$	530.61	2_2^+	1	1	
		1175.57	$\mathbf{2_1^+}$	0.10	0.05 (1)	
2104.66	$\mathbf{3_1^+}$	594.65	4_1^+	0.66	<0.40[a]	
		672.50	2_2^+	1	1	$+6.66^{+3.41}_{-1.71}$
		1317.37	$\mathbf{2_1^+}$	0.13	0.04 (3)	$+2.91^{+0.64}_{-0.46}$
2223.74	$\mathbf{4_2^+}$	713.80	4_1^+	1	1	+1.13 (17)
		791.58	2_2^+	1.60	0.88 (11)	
		1436.68	$\mathbf{2_1^+}$	0.03	0.04 (1)	
2419.48	$\mathbf{4_4^+}$	661.16	$\mathbf{2_3^+}$	1	1	
		909.52	4_1^+	0.54	0.33 (3)	−0.64 (10)
		1632.46	$\mathbf{2_1^+}$	0.06	0.02 (1)	

[a] Branching ratio adopted from Ref. [23], no multipole mixing ratio available, assumed to be a pure E2 transition.

are almost equally mixed with fraction of 55.3% and 46.9%, respectively.

One should also notice that the unperturbed normal and the intruder level schemes exhibit, to a certain extent, vibrational and γ-soft characteristics, respectively. Within the unperturbed intruder configuration, the $R_{4/2} = E(4_1^+)/E(2_1^+)$ ratio of 2.67, as well as the closely lying 4_1^+, 2_2^+ states, in which a two-phonon 0^+ state is absent, is typical for a γ-soft structure. The unperturbed normal configuration, in contrast, displays closely lying 4_1^+, 2_2^+, and 0_2^+ states, more typical for a spherical vibrator. Also the $R_{4/2} = 2.32$ of the unperturbed normal configuration deviates strongly from deformed values toward the spherical harmonic oscillator ($R_{4/2} = 2.0$). This interpretation correlates with the microscopic energy surface in Fig. 4(a) and is consistent with previous empirical IBM-2 fitting calculations [46].

Finally, in Tables II and III we compare experimental and theoretical B(E2) values. Lifetimes are either adopted from Ref. [14] or measured in the present experiment. If not stated differently, all multipole mixing ratios and branching ratios are from the present work. The conversion coefficient α was obtained from calculations using the code BRICC [47]. Very good agreement between experiment and theory is obtained, confirming the strong mixing between both configurations. In particular, the strong $B(\mathrm{E2}; 2_1^+ \to 0_2^+)$ and $B(\mathrm{E2}; 2_2^+ \to 2_1^+)$ transitions, relative to the $2_1^+ \to 0_1^+$ transition (see Table II), present a stringent test of configuration mixing. The measured $B(\mathrm{E2}; 6_1^+ \to 4_1^+)$ is much smaller than predicted, perhaps due to fragmentation.

In Table III we compare relative B(E2) values, normalized with respect to the largest B(E2) value among the depopulating decays from a given initial state, for the states without lifetime information. Note that the three $4^+_{2,3,4,\mathrm{expt}}$ states are observed within 200 keV. From comparison of relative B(E2) values the $4^+_{2,\mathrm{expt}}$ state can be assigned to the predicted $4^+_{3,\mathrm{theor}}$ state generated mainly by the intruder configuration, while the $4^+_{4,\mathrm{expt}}$ state can be assigned to a strongly mixed $4^+_{2,\mathrm{theor}}$ state. Table III shows the same extent of consistency as obtained in Table II.

V. CONCLUSION

We have revealed robust experimental evidence for shape coexistence and configuration mixing in the low-lying structure of ^{98}Mo. Key data on multipole mixing ratios and lifetimes have been obtained, allowing for a detailed comparison with a new theoretical calculation within the IBM based on the microscopic EDF. The EDF calculation predicted two (near-spherical and γ-soft) mean-field minima in the energy surface [Fig. 4(a)], which necessitates the extension of the IBM to include a intruder configuration associated with the proton excitation across the $Z = 40$ subshell closure. The two intrinsic shapes are mixed strongly into low-spin states (cf. Fig. 5). The excitation spectra and E2 properties are calculated in a fully microscopic way and are in excellent agreement with the wealth of new spectroscopic data and consistent with a previous phenomenological IBM fit [46]. The theoretical method used in this work is robust and capable of appropriately modeling the coexistence of different shapes. Hence, it allows for a universal description of nuclear shapes and will be applied to other heavy exotic nuclei in the future.

ACKNOWLEDGMENTS

We thank the Tandem accelerator staff at the Wright Nuclear Structure Laboratory, Yale University for their help during the experiment. This work is supported by US DOE under Grant No. DE-FG02-91ER-40609. K.N. acknowledges the support through the JSPS postdoctoral program for research abroad. P.P. is indebted to the Bulgarian Science Fund for the financial support under contract DFNI-E 01/2.

[1] J. L. Wood, K. Heyde, W. Nazarewicz, M. Huyse, and P. van Duppen, Phys. Rep. **215**, 101 (1992).
[2] K. Heyde and J. L. Wood, Rev. Mod. Phys. **83**, 1467 (2011).
[3] G. E. Brown and A. M. Green, Nucl. Phys. **85**, 87 (1966).
[4] A. N. Andreyev *et al.*, Nature (London) **405**, 430 (2000).
[5] W. Nazarewicz, Phys. Lett. B **305**, 195 (1993).
[6] V. Werner *et al.*, Phys. Lett. B **550**, 140 (2002).
[7] G. S. Simpson *et al.*, Phys. Rev. C **74**, 064308 (2006).
[8] P. Cejnar, J. Jolie, and R. F. Casten, Rev. Mod. Phys. **82**, 2155 (2010).
[9] A. Chakraborty *et al.*, Phys. Rev. Lett. **110**, 022504 (2013).
[10] K. Sieja, F. Nowacki, K. Langanke, and G. Martinez-Pinedo, Phys. Rev. C **79**, 064310 (2009).
[11] P. Federman and S. Pittel, Phys. Rev. C **20**, 820 (1979).
[12] G. Rusev *et al.*, Phys. Rev. Lett. **95**, 062501 (2005).
[13] D. Burch, P. Russo, H. Swanson, and G. E. Adelberger, Phys. Lett. B **40**, 357 (1972).
[14] M. Zielinska *et al.*, Nucl. Phys. A **712**, 3 (2002).
[15] F. Iachello and A. Arima, *The Interacting Boson Model* (Cambridge University Press, Cambridge, 1987).
[16] C. W. Beausang *et al.*, Nucl. Instrum. Methods Phys. Res., Sect. A **452**, 431 (2000).
[17] K. S. Krane and R. M. Steffen, Phys. Rev. C **2**, 724 (1970).
[18] K. S. Krane, R. M. Steffen, and R. M. Wheeler, At. Data Nucl. Data Tables **11**, 351 (1973).
[19] I. Wiedenhöver, code CORLEONE, University of Cologne, 1995 (unpublished).
[20] I. Wiedenhöver *et al.*, Phys Rev. C **58**, 721 (1998).
[21] M. E. Rose, Phys Rev. **91**, 610 (1953).
[22] R. J. Casperson, Ph.D. thesis, Yale University, 2009 (unpublished).
[23] B. Sing, Nucl. Data Sheets **98**, 335 (2003).
[24] E. Williams *et al.*, Phys. Rev. C **80**, 054309 (2009).
[25] R. A. Meyer, J. Lin, G. Molnar, B. Fazekas, A. Veres, and M. Sambataro, Phys. Rev. C **29**, 1839 (1984).
[26] W. M. Currie and C. H. Johnson, Nucl. Instrum. Methods **63**, 221 (1968).
[27] L. C. Northcliffe and R. F. Schilling, At. Data Nucl. Data Tables **7**, 233 (1970).
[28] J. F. Ziegler, *Helium Stopping Powers and Ranges in Elemental Matter* (Pergamon Press, New York, 1978).
[29] P. Petkov *et al.*, Nucl. Phys. A **640**, 293 (1998).
[30] M. Bender, P.-H. Heenen, and P.-G. Reinhard, Rev. Mod. Phys. **75**, 121 (2003).

[31] A. Bohr and B. R. Mottelson, *Nuclear Structure* (Benjamin, New York, 1975), Vol. II.
[32] E. Chabanat, P. Bonche, P. Haensel, J. Meyer, and R. Shaeffer, Nucl. Phys. A **627**, 710 (1997).
[33] P. Bonche, H. Flocard, and P.-H. Heenen, Comput. Phys. Commun. **171**, 49 (2005).
[34] T. Otsuka, A. Arima, and F. Iachello, Nucl. Phys. A **309**, 1 (1979).
[35] J. N. Ginocchio and M. W. Kirson, Nucl. Phys. A **350**, 31 (1980).
[36] K. Nomura, N. Shimizu, and T. Otsuka, Phys. Rev. Lett. **101**, 142501 (2008).
[37] K. Nomura, R. Rodríguez-Guzmán, L. M. Robledo, and N. Shimizu, Phys. Rev. C **86**, 034322 (2012).
[38] M. Albers *et al*., Nucl. Phys. A **899**, 1 (2013).
[39] P. D. Duval and B. R. Barrett, Phys. Lett. B **100**, 223 (1981).
[40] A. Kankainen *et al*., J. Phys. G **39**, 093101 (2012).
[41] K. Nomura, N. Shimizu, D. Vretenar, T. Niksić, and T. Otsuka, Phys. Rev. Lett. **108**, 132501 (2012).
[42] P. Paradis, R. Lecomte, S. Landsberger, and S. Monaro, Phys. Rev. C **20**, 1201 (1979).
[43] R. J. Peterson, R. A. Emigh, and R. E. Anderson, Nucl. Phys. A **290**, 155 (1977).
[44] G. M. Ukita, T. Borello-Lewin, L. B. Horodynski-Matsushigue, J. L. M. Duarte, and L. C. Gomes, Phys. Rev. C **64**, 014316 (2001).
[45] J. Barrette, M. Barrette, A. Boutard, R. Haroutunian, G. Lamoureux, and S. Monaro, Phys. Rev. C **6**, 1339 (1972).
[46] M. Sambataro and G. Molnár, Nucl. Phys. A **376**, 201 (1982).
[47] T. Kibédi, T. W. Burrows, M. B. Trzhaskovskaya, P. M. Davidson, and C. W. Nestor, Nucl. Instrum. Methods Phys. Res., Sect. A **589**, 202 (2008).